ornl

OAK
RIDGE
NATIONAL
LABORATORY

UNION
CARBIDE

ORNL/TM-7552

Approach to Ignition of Tokamak Reactors

D. J. Sigmar

OPERATED BY
UNION CARBIDE CORPORATION
FOR THE UNITED STATES
DEPARTMENT OF ENERGY

ORNL/TM-7552
Dist. Category UC-20g

Contract No. W-7405-eng-26

FUSION ENERGY DIVISION

APPROACH TO IGNITION OF TOKAMAK REACTORS

D. J. Sigmar*

Material used here contributed by

ORNL	PPPL
W. A. Houlberg	C. Singer et al.
H. C. Howe	D. Post
K. T. Tsang	D. Mikkelsen
Y-K. M. Peng	
Computer Sciences Division Staff	

NOTICE This document contains information of a preliminary nature. It is subject to revision or correction and therefore does not represent a final report.

Date Published - February 1981

*Fusion Energy Division at ORNL and Nuclear Engineering Department at MIT.

Prepared by the
OAK RIDGE NATIONAL LABORATORY
Oak Ridge, Tennessee 37830
operated by
UNION CARBIDE CORPORATION
for the
DEPARTMENT OF ENERGY

CONTENTS

1. INTRODUCTION

Over the last few years an increasing stream of individual tokamak physics results has been forthcoming, e.g., $n\tau$ in Alcator, T_i in PLT, β in ISX, etc. During the same period semiempirical numerical models for basic plasma processes have been constructed, and the results have strengthened our belief that heating to ignition is attainable in a device on the scale of the Engineering Test Facility (ETF). In ETF we will attempt to meet ignition and plasma burn control requirements simultaneously. Although it is by no means straightforward to simulate definitively the multitude of interacting processes, we assemble here what is considered known about confinement and ignition (and a certain feature of alpha particle dynamics) and what some of the design margins may be for the present choice of ETF parameters. We shall do this with a critical look for large extrapolations, for the validity of underlying assumptions, and for the high-leverage physics issues.

Figure 1 shows a typical time history of T_i and n_e on the way to ignition in ETF, as modeled by Houlberg et al.[1] It seems that ignition is reached at $\beta \cong 4\%$, after $\cong 6$ s of neutral beam heating. The rest of this paper discusses some obvious and hidden uncertainties that arise when one incorporates many individual, extensive subroutines describing beam heating, fueling, cross-field transport of electrons, fuel ions, alphas and impurities and ensuing radiation, plasma-wall interactions, divertor models, etc.

It is difficult to make the necessary simplifications and approximations uniformly and self-consistently in all places. For example, a (necessarily) strongly simplified impurity transport model can result in large uncertainties in the radiation profile. This produces the same uncertainties for $T_e(r)$ and thus for the current density and pressure profile (both sensitively affecting ideal and resistive MHD stability at high beta), the neoclassical impurity screening, the divertor efficiency, and therefore the impurity source rate, which closes the cycle of indeterminancy in predicting ignition. This was reflected in a recent European meeting on beam requirements for JET (see Table 1). However, experiments will continue to provide benchmarks for the developing

Table 1. Previous predictions for JET[a] (extended performance with 45 MW at 160 keV)

	No impurities	With impurities		
Code	Result	Source of impurity	Transport	Result
Duechs	Near ignition	Neutral particle sputtering	Neoclassical (with $\partial T/\partial r$ screening + $\chi_e/4$)	No ignition
Watkins/Gibson	Ignition	Ion plus neutral sputtering	Neoclassical (without $\partial T/\partial r$ screening)	No ignition
Mercier	Ignition	Fixed percent of impurity		Ignition if f < 0.2% of iron
Hughes/Ashby	Ignition	Neutral particle sputtering	Neoclassical (with $\partial T/\partial r + \chi_e/4$)	Ignition

[a]From "US/EC Meeting on Neutral Beam for D-T Machines," Varenna, September 1979.

transport modeling. In this situation it follows that a continued focused effort in tokamak experiments (ISX, PDX, TFTR, JET) and theory and transport modeling by independent groups will be essential for a sound design for ETF.

The rest of this paper will deal briefly with JET modeling (Sect. 2), INTOR modeling (Sect. 3), ETF modeling (Sect. 4), and a model of anomalous alpha particle transport (Sect. 5). Conclusions for the present ETF design are included in the last section. It should be pointed out that ideal and resistive MHD stability considerations have not yet been integrated with the transport modeling results in this paper.

2. JET MODELING

We briefly discuss the recent results by M. L. Watkins et al. on the approach to ignition in large tokamaks.[2] Major parameters are given in Table 2. Figure 2 shows ignition boundaries in $\bar{n}a$ versus β^* space for four different electron scalings: (A) $\chi_e = K_1/n$; (B) $\chi_e = K_2/nT_e$; (C) $\chi_e = K_3\sqrt{T_e}/nqR$; and (D) $\chi_e = (K_4/n)(1 - r^2/a^2)^{3.5}$. Note the factor 2 variations in β^*_{ig} and $\bar{n}a$ for the different confinement models, perhaps implying serious design changes. Note also that the density at the minimum β^*_{ig} tends to be below 10^{14} cm^{-3} for all scalings. We will return to this in Sect. 3. Figure 3 shows the same parameter space for scaling (A) and 160-keV D^0 injection. One notes the existence of a saddle point on the surface of the injection power required for power balance (the curves are labeled with the injection power in megawatts). This shows that a variable-density startup[3] path exists across the saddle along which beam power is minimal. Experimentally verified knowledge of this path would clearly be of great design relevance. Figure 4 shows a constant density cut through the landscape of Fig. 3, demonstrating again the large effect of χ_e scaling on ignition capability, in this case beam power. Figure 5 accentuates the uncertainty in impurity modeling by showing a doubling of required beam power for ignition for modest amounts of impurities.

A 50% beam power margin capability suggests itself from these studies; this may be easier to accommodate than a variable minor plasma

Table 2. Machine parameters

	JET	INTOR (1979)	ETF (1980)
R, m	2.96	4.8	5.4
$\sqrt{ab}$, m	1.62	1.47	1.64
b/a	1.7	1.5	1.6
$B_T(0)$, T	3.45	5	5.5
Percent of coils		12	10
Typical $\langle n_e \rangle$, m^{-3}	1×10^{20}	1.4×10^{20}	1×10^{20}
Fueling	Gas puff	Gas puff	Pellets
Beam current		0.6/0.24/0.16	0.53/0.25/0.22
Beam power	0.58/0.23/0.19		0.73/0.17/0.10
Beam tangency radius, m		1.63	3.55

radius. Figure 6 depicts ignition parameters as before, plus the time needed to get to a certain point with the basic (17.5-MW) or extended performance (45-MW) beam power system for JET. The number in parentheses is roughly P_α/P_{loss}, 1.0 being ignition. Probably the most ETF-relevant branch is the extended performance, $\chi_e \sim 1/N$ model, impure solid branch II showing attainment of 80% of ignition and $T_o \cong 29$ keV after 5 s but failure to ignite because of impurities. This will be corroborated in the next section.

In summary, these JET studies show (1) significant sensitivity of β_{ig} and P_{beam} to factor 2 variations in electron heat conductivity; (2) the existence of a minimum beam power path to ignition using a variable density approach and favoring densities below or at 10^{14} cm^{-3}; (3) the need for a 50% beam power margin to compensate for impurity radiation; and (4) the possibility that, depending on rather modest possible variations of electron confinement scaling and impurity concentration, full ignition may not occur.

3. INTOR MODELING

We briefly discuss work by C. Singer et al.[4] using the January 1979 INTOR parameters shown in Table 2. Figure 7 shows ignition at $\beta_{total} = 5\%$ and its components for fixed impurities with $Z_{eff} = 1.5$. Figure 8 shows again the substantial sensitivity of β_{ig} and t_{ig} on a possible factor 3 variation of χ_e/n_e. A resulting threefold increase of t_{ig} would constitute a severe beam system design change. A 50% margin capability for t_{ig} seems indicated. A very interesting idea to ensure the design against a 2.5-fold uncertainty of χ_e is shown in Fig. 9. By varying the minor plasma radius according to $a^2 \propto \chi_e$, the increase in size (and various other parameters so that beam power density, etc., is kept constant) compensates for deteriorating electron confinement χ_e. Note that in this way β_{ig} and t_{ig} can be kept at acceptable levels. A possible 2.5-fold increase in χ_e cannot be ruled out in view of the fact that even the highest volume-averaged (not peak) ion temperatures achieved in PLT are almost an order of magnitude lower than the optimal reactor burn average temperatures. Note also (at the bottom of Fig. 9)

that, with the second case the standard INTOR size and the third close to ETF (see Table 2), ETF appears to have a substantial ignition margin over this INTOR design, provided that standard INTOR scaling for χ_e applies. From this study it appears that a variable minor radius capability would be desirable.

Figure 10 shows the effect of heavy metal impurities on the attainment of ignition. Similar to the JET modeling results, $t_{ig} \to \infty$ for rather modest impurity concentrations. Quantitatively these one-dimensional (1-D) transport calculations confirm previous 0-D fatal impurity fraction[5] estimates to within a factor of 2. Figure 11 demonstrates quench at $\geq$2% nickel, and Fig. 12 shows the critical impurity fraction (where radiation equals the beam power input) versus atomic number. Radiation losses dominate conduction losses so much that increasing the minor radius $a \to \infty$ is ineffective. The figure also shows an independent result by H. Howe.[6]

Figure 13 deals with the dependence of the steady-state helium fraction f_{He} on the helium-pumping rate at the edge. A long-pulse ($t \geq 15$ s) simulation is needed to reach the ignition quench becaue of helium ash accumulation. For the long-pulse simulations Singer et al. add several effects to the code such as thermal ripple losses with 1% edge ripple, charge exchange of fast ions on hydrogen, scrape-off layer and recycling, etc. The figure shows a 0.5% edge pumping fraction to be sufficient with very little reduction of f_{He} beyond that. This is due to the dominant helium recycling at the edge.[7]

In summary, these INTOR studies show (1) ignition occurs at β_{ig} = 4-5%, t_{ig} = 7 s with a flat, constant, low Z impurity density at Z_{eff} = 1.5; (2) β_{ig} and t_{ig} (and beam power and pulse length) are a strong function of χ_e (at densities of $\cong 10^{14}$ cm^{-3} a factor of $\leq$3 enhancement of χ_i over $\chi_{i\ neoclassical}$ does not matter very much, however); (3) β_{ig} can be kept in the 4% range if a minor radius increase according to $a^2 \propto \chi_e$ is designed should χ_e increase with the needed tenfold increase from present PLT values of volume-averaged ion temperature to steady-state burn temperatures; (4) fatal metal impurity concentrations from this 1-D simulation agree roughly with previous 0-D predictions (an increase in minor radius is quite incapable of increasing these fatal fractions);

and (5) a 1% edge ripple permits ignition, and a 0.5% helium-pumping fraction suffices to avoid quench due to alpha particle ash in long-pulse simulations.

4. ETF MODELING

ETF transport modeling work has recently been carried out at Oak Ridge National Laboratory (ORNL) and Princeton Plasma Physics Laboratory (PPPL). The ORNL work by W. Houlberg et al.[1] on the bundle divertor version of ETF deals with ignition startup (variable density and fuel mix), particle and energy flux balance to walls and divertors, and sensitivity of the fusion alpha power to fast-particle losses. The present emphasis is on the increasing realism and self-consistency of the various subprocesses involved in the transport codes reflected in the development of

(1) self-consistent, time-dependent sputtering rates (impurity sources),
(2) a detailed recycle model for deuterium, tritium, *and* helium, distinguishing between recycling on the wall and recycling from the divertor,
(3) tritium lean pellet fueling scenarios, and
(4) sensitivity of fusion power to thermal ions and fast-alpha bananas.

At PPPL work on the poloidal divertor version of ETF by D. Mikkelsen et al.[8] has begun on state-of-the-art ripple loss modeling of beam ions and alpha particles. An investigation of neutral beam ion confinement for varying injection angles shows that the design value of 16° away from perpendicular provides adequate fast-ion confinement, to be discussed below.

4.1 ETF BASE CASE WITH BUNDLE DIVERTOR

Figure 14 shows the temperature and density evolution during fusion startup in ETF. Ignition occurs at $\langle\beta\rangle \cong 4\%$. The transport equations used are given in Table 3. The model for χ_e is the PLT model (D) defined

Table 3. Plasma transport model for ETF base case
(W. Houlberg et al.)

$$\Gamma_j = \Gamma_j^{neo} - D^{an} \frac{\partial n_j}{\partial r} \qquad j = D,T,\alpha; \qquad \Gamma_e = \Sigma\, Z_j \Gamma_j$$

$$q_j = q_j^{neo} - \chi_j^{ripple}\, n_j \frac{\partial T_j}{\partial r}$$

$$q_e = -\chi_e^{an}\, n_e \frac{\partial T_e}{\partial r}$$

$$D_j^{an} = \frac{1.25 \times 10^{17}}{n_e} + 5000(r/r_s)^3$$

$$\chi_e^{an} = \frac{1 \times 10^{17}}{n_e[1 - 0.4(r/r_s)^2]^{3.5}}$$

χ_i^{ripple} ... Uckan, Uckan, and Moore, ORNL/TM-5603 (1976). Including noncircular cross section; not including ripple plateau diffusion.

by Watkins[2] in Sect. 2. Its radial increase of χ_e leads to strongly peaked profiles with $T(0) \cong 2\langle T\rangle$ [see Fig. 14(a)]. Beam heating lasts for 6 s; a thermal steady state is reached due to ripple losses for T_i and mainly conduction and radiation losses for T_e. The radial profiles for T_i and T_e in Fig. 14(b) are at t = 20 s when $\langle\beta_{total}\rangle \cong 6.8\%$ and $\langle\beta_{\alpha,fast}\rangle \cong 2\%$. These rather high values follow from the rather low values of density [see Figs. 14(c) and (d)], the small ripple losses, and the absence of impurities. The behavior of $n_e(0)$ in Fig. 14(c) reflects pellet fueling. Note in Fig. 14(d) that a delayed lean tritium fueling scenario has been chosen to minimize neutron loads on the beam injection system but that the result is still high fusion power output (see below).

The chosen value for $\langle\bar{n}_e\rangle \cong 10^{14}$ cm^{-3} raises a question with respect to the Murakami limit. Figure 15, taken from recent DITE experiments,[9] is reassuring in this respect, showing that the original density limit in ohmically heated tokamaks is substantially extendable by auxiliary (and presumably also alpha particle) power. The value of (B_ϕ/R) is very similar for DITE and ETF, suggesting that a mean density of 10^{14} cm^{-3} should be achievable.

Figure 16 shows the particle balance for this ETF base case with a bundle divertor. Charged particles hitting the wall [Fig. 16(a)] are assumed to fully recycle as neutrals. The neutral flux to the wall is approximately half the charged particle flux [Fig. 16(b)]. Charge exchange neutrals are reflected according to the Oen-Robinson[10] wall reflection model, partly as hot, partly as thermal, neutrals. The ion flux to the divertor is shown in Fig. 16(c), assuming zero divertor recycling. Particle pumping efficiencies for deuterium, tritium, and alphas are listed in the figure.

Figure 17 shows the energy balance. Figure 17(a) contains bremsstrahlung (and synchrotron radiation) but no impurity radiation, an omission reflecting the present uncertainties in self-consistent impurity source transport modeling. (Work on this has started, however.) Similarly underestimated is the amount of charged particle energy flux to the wall [Fig. 17(b)], again omitting the contribution from impurities. The charge exchange and ionization power losses are given in Fig. 17(c) and the power deposition to the divertor plates in Fig. 17(d). The

corresponding divertor energy pumping efficiencies are given in Fig. 18, together with the total fusion and alpha power output for this case.

The plasma parameters for burn can be substantially altered over a wide range if burn control by variable toroidal field ripple can be assumed. An effect of increased ripple is to suppress T_i relative to T_e. The plasma density can then be increased to retain similar values of fusion power and plasma beta. The increased fueling (by pellet) can substantially increase the density and decrease the temperature in the bundle divertor scrape-off region, resulting in a dramatic reduction in the wall power load via charge exchange neutrals. The results of these calculations are summarized in Table 4.

It is seen that for a constant fusion power (P_α = 150 MW) via burn control, $\langle T_i \rangle$ can vary from 23 to 7 keV, β_{total} from 7.3 to 4.9%, P_{rad} (in the absence of impurities) from 6.6 to 22.5 MW, and P_{cx} from 24.6 to 1.5 MW as $\langle n_i \rangle$ is varied from 0.8×10^{14} to 2.0×10^{14} cm^{-3}. Power into the divertor and on the limiter (first wall) via charged particles remains relatively unchanged. It should be noted that the ripple magnitude (δ_{edge}) indicated in Table 4 is based on Stringer's model of ion heating conduction enhanced by ripple trapping. More detailed modeling of ripple effects is expected to result in reduced values of δ_{edge} required for burn control. It is by no means clear which of the three areas indicated in Table 4 is more nearly optimal.

We next present results on the effect of plasma current on the ripple losses and, therefore, on fusion power and temperatures. Although the empirical or INTOR electron energy confinement scaling is independent of plasma current (although Coppi-Mazzucatto claim otherwise), ripple enhancement of ion heat conduction depends on the current through the flux geometry form factor $G(\alpha)$. For circular cross section $G(\alpha)$ is inversely proportional to the safety factor. For general flux geometry one obtains a more complicated dependence on the poloidal field and, thus, the current.[11] Table 5 shows the sizable effect on the fusion power of dropping the current from 5 to 4 MA. Note also the drop in peak ion temperature and a flattening of $T_i(r)$ due to increased ripple conduction losses.

Table 4. Plasma burn parameters and power loads for various plasma densities in a bundle divertor ETF with a = 1.3 m, Δ (scrape-off) = 0.1 m, R_o = 5.4 m, σ = 1.6, I_p = 5 MA, B_T = 5.5 T and assuming ripple burn control to maintain P_α = 150 MW

	Low N	Medium N	High N
$\langle n_i \rangle$, 10^{14} cm^{-3}	0.85	1.5	2.0
δ_{edge}, %	±1.0	±3.3	±5.4
$\langle T_i \rangle$, keV	23.0	9.5	7.0
$\langle T_e \rangle$, keV	24.8	13.8	9.3
$\bar{\beta}_{plasma}$, %	5.5	4.7	4.4
$\bar{\beta}_{total}$, %	7.3	5.6	4.9
S_{pellet}, number/s	29	52	62
$n_{He}(0)$, 10^{13} cm^{-3}	0.7	1.5	2.0
P_{div}, MW	70.5	90.0	88.8
P_{lim}, MW	46.0	43.7	39.5
P_{rad}, MW	6.6	10.4	22.5
P_{cx}, MW	24.6	5.0	1.5

Table 5. Effects on power balance of changing plasma current and therefore ripple losses

	I = 5 MA (base case)	I = 4 MA
P_{total}	835	750
P_{α}	167	150
$T_i(0)$	52.5	44
$\langle T_i \rangle$	26.4	22.7
$T_e(0)$	63.4	59.7
$\langle T_e \rangle$	28.5	26.2

Because there are strong indications that the ripple due to a bundle divertor is too large to confine the fast-alpha bananas,[12] the effect of eliminating the trapped fraction $(2r/R)^{1/2}$ of all energetic alpha particles from the burn was studied. Table 6 shows the expected strong 50% drop in P_α but only a 19% drop in P_{total}. However, the remaining alpha power is still larger than the beam power originally used to reach ignition. One concludes that this loss of trapped alpha particles is tolerable from an energy perspective but still must be evaluated in terms of blistering and impurity production.

4.2 ETF BASE CASE WITH POLOIDAL DIVERTOR

One of the most significant differences between bundle and poloidal divertors lies in the reduction of ripple losses and, therefore, the possibility of more perpendicular neutral beam injection. Figure 19 shows injection at 2.5° from vertical.[8] Beam ion banana tips lie entirely in the symmetric trapping region and are thus subject to strong ripple losses. δ_o is the ripple strength parameter in the assumed ripple model

$$\delta(R,z) = \delta_o \exp\{[(R - R_1)^2 + Z^2]^{1/2}/\lambda\} .$$

Figure 20 shows the remarkable improvement at an injection angle of 16°, the design value. Figure 21 contains a summary of complete injection heating simulations for various sets of plasma parameters (denoted by P1, P2, P3, and P4, with P1 being the standard ETF design case) and various values of safety factor q (see insert in Fig. 21). The lower four curves show the expected behavior of beam power loss with the injection angle at 0.75% edge ripple and clearly favor low q operation for the purpose of good orbit confinement, possibly in conflict with profile requirements to avoid MHD instabilities. The attainable beam power coupling to the plasma appears high. The upper two curves in Fig. 21 were run with a deliberately high edge ripple of 4.5%, showing intolerable beam power losses, as expected.

The conclusions on ETF modeling will be given in the last section of this paper.

Table 6. Effect of losing all fast-alpha bananas $\propto \sqrt{2\varepsilon}$

	Before losing	After losing
P_{total}	835	679
P_{α}	167	136 → 68.3
$T_i(0)$	52.5	48.8
$\langle T_i \rangle$	26.4	20.7
$T_e(0)$	63.4	52.3
$\langle T_e \rangle$	28.5	19.7

5. ANOMALOUS ALPHA PARTICLE TRANSPORT

The two main questions regarding the dynamics of alpha particles are their anomalous relaxation in velocity space, possibly leading to anomalous fuel ion heating, and their anomalous radial transport from the center to the edge, where the helium ash can be pumped. Kolesnichenko has recently reviewed the role of alpha particles in tokamak reactors.[13] Here we report a new development regarding their radial outward diffusion.

Sigmar, Tsang, and Whitson[14] have shown that the low mode number Alfvén wave can exist with a discrete spectrum of radial eigenmodes in a tokamak with sheared magnetic field. A complete numerical computation of the spectrum reveals that radially neighboring resonances $\omega^2 = C_A^2 k_\parallel^2$ are spaced so narrowly (e.g., ≅3 cm) for fixed m = 2, ℓ = 3 or m = 3, ℓ = 4 that island overlap of the perturbed alpha particle orbits in action-angle space occurs at very small threshold amplitudes $e_i\phi/T_i \cong 0.05$ of the enhanced Alfvén fluctuations in the fusion plasma. Evaluating the stochastic diffusion coefficient at this threshold, one obtains for the fast alphas [with $v_\alpha > c_A$ (the Alfvén velocity)]

$$D_{rr}^{\alpha} \cong 4.4 \times 10^3 \text{ cm}^2/\text{s}, \quad \tau_\alpha = (a^2/2)D_{rr}^{\alpha} = 1.1 \text{ s} .$$

Note that this alpha particle confinement time is longer than the slowing-down time but shorter than the estimated main particle confinement time, thus guaranteeing alpha particle heating yet rapid ash removal from the burning center. It should be mentioned that although the authors are satisfied with the exact calculation of the linear spectrum, the estimate of D_{rr}^{α} is preliminary. The difficulties of a self-consistent nonlinear transport theory for driftlike waves (driven in this case by the alpha particle density gradient) are well known, and it remains for the experiment to check this prediction. Because without effective ash removal the ETF fusion burn would quench in 20-25 s, it is very important to obtain experimental data on the behavior of fast alpha particles in TFTR, as has been suggested by D. Post et al.,[15] using a 6-MeV lithium doping beam, charge exchanging with alpha particles in the reaction

$$He^{2+} + Li^{0} \rightarrow He^{0} + Li^{2+} ,$$

shown schematically in Fig. 22.

6. CONCLUSIONS

This brief review of recent transport simulations of JET, INTOR, and ETF leads one to the following observations for the consideration of an ETF design.

(1) The present ETF design parameters permit ignition at $\langle\beta\rangle \cong 4\%$ after 6-7 s of neutral beam heating if a very simplified impurity model is used and assuming the fatal fractions of heavy impurities have not been reached. Automatic ripple burn control then leads to a thermal steady state with 1-2-MW/m^2 neutron wall loading.

(2) Several issues of previous concern have been cleared up; e.g.:
   (a) There exists a variable-density startup path with minimal beam power requirements.
   (b) The Murakami density limit is extendable by beam (and perhaps by alpha) power; $\langle n_e \rangle \gtrsim 10^{14}$ cm^{-3} appears to be attainable.
   (c) The ten-coil design with $\leqslant 1\%$ edge ripple is tolerable.
   (d) A 16° injection angle is acceptable for the poloidal divertor design, and 35° is acceptable for the bundle divertor design (with two T-shaped coils, suggested by T. Yang).
   (e) A loss of all banana-trapped alpha particles is tolerable with respect to the overall power balance.
   (f) Helium pumping $\geqslant 0.5\%$ at the edge is sufficient to avoid quenching of the burn. Theoretical estimates yield sufficiently large anomalous outward diffusion of fast-alpha particles to transport the helium ash to the edge.
   (g) Burn control occurs automatically as a result of a combination of ripple losses and density control.

(3) Although getting into better focus, several sensitive areas affecting ignition remain. These include the following:
   (a) One area is the self-consistent analysis of long-pulse impurity generation and transport with and without divertor modeling.

(b) As part of this, there exist maximum allowable values for the increase in n_z/n_e for all impurity species Z and for dZ_{eff}/dt and the impact on required beam power and pulse-length margins.

(c) Because $\langle T_i \rangle$ will increase by a factor of 5-10 from present values (in PLT) to reactor values, a factor of 2 increase in χ_e is conceivable. Then to stay within the range of $\beta_{ig} \cong 4\%$ and $t_{ig} \leq 7\text{-}10$ s would require a minor radius margin capability of $\sqrt{2}$, or a corresponding margin in beam capability to run ETF as a wet-wood burner.

(d) Good beam and alpha particle confinement against ripple losses favors operation at low safety factor, which may be incompatible with other profile shaping requirements not discussed here.

In closing, two overall impressions should be mentioned. One is the suggestion to continue to explore design variations, particularly at a lower magnetic field and higher beta (mainly at similar densities and higher temperatures). The other is to state that the attainment of the minimum physics objective of ETF, namely, obtaining operation with alpha power dominating the power balance at least in the inner half of the volume, must be protected by approximate design margins, particularly in the auxiliary heating system, and by the possibility of plasma parameter and profile control. As a corollary, even if it were possible to produce one certain cost-optimized ETF design, this would yield only one data point of fusion device, and the next-generation demonstration reactor might have to carry the burden of exploring the deviations from this one point.

REFERENCES

1. W. A. Houlberg (Oak Ridge National Laboratory), private communication, 1980 (to be published).
2. M. L. Watkins, T. E. Stringer, A. Gibson, W. G. F. Core, I. L. Robertson, J. G. Cordey, and J. J. Field, paper presented at the *8th Int. Conf. on Plasma Physics and Controlled Nuclear Fusion Research*, IAEA-CN-38/W-3, Brussels, 1980.
3. J. A. Holmes, J. A. Rome, W. A. Houlberg, Y-K. M. Peng, and S. J. Lynch, Nucl. Fusion 20, 59 (1980).
4. C. E. Singer, F. G. Seidl, D. E. Post, and P. H. Rutherford, PPPL-1693, Princeton, New Jersey (1980).
5. R. V. Jensen, D. E. Post, and D. L. Jassby, Nucl. Sci. Eng. 65, 282 (1978).
6. H. C. Howe (Oak Ridge National Laboratory), private communication, 1980 (to be published).
7. C. E. Singer, F. G. Seidl, D. E. Post, and P. H. Rutherford, PPPL-1693, Princeton, New Jersey (1980); H. C. Howe (Oak Ridge National Laboratory), private communication, 1980.
8. D. R. Mikkelsen (Princeton Plasma Physics Laboratory), private communication, 1980.
9. S. K. Erents, S. J. Fielding, R. D. Gill, D. H. J. Goodall, J. Hugill, G. M. McCracken, J. E. Partridge, J. W. M. Paul, B. A. Powell, R. Prentice, G. Proudfoot, A. D. Sanderson, J. H. Shea, C. Sofield, D. D. R. Summers, J. E. Vince, and A. J. Wootton, paper presented at the *8th Int. Conf. on Plasma Physics and Controlled Nuclear Fusion Research*, IAEA-CN-38/X-3, Brussels, 1980.
10. O. S. Oen and M. T. Robinson, Nucl. Instrum. Methods 132, 647 (1976).
11. R. J. Goldston and H. H. Towner, Nucl. Fusion 20, 781 (1980).
12. L. M. Hively, J. A. Rome, and V. E. Lynch, Bull. Am. Phys. Soc. (to be published).
13. Y. I. Kolesnichenko, Nucl. Fusion 20, 727 (1980).
14. K. T. Tsang, D. J. Sigmar, and J. C. Whitson, ORNL/TM-7508, Oak Ridge, Tennessee (to be published).
15. D. E. Post, D. R. Mikkelsen, R. A. Hulse, L. D. Stewart, and J. C. Weisheit, PPPL-1592, Princeton, New Jersey (1979).

FIGURE CAPTIONS

Fig. 1. Ion temperature and electron density in ETF as a function of radius and time (from Ref. 1).

Fig. 2. Generalized Lawson diagram for various scaling laws as described in the text (from Ref. 2).

Fig. 3. Generalized Lawson diagram with contours of constant beam power in megawatts. Note the path to ignition across the saddle point (from Ref. 2).

Fig. 4. A cross section of the contour map of Fig. 3 showing beam power needed vs ion temperature for the different scaling laws of Fig. 2 (from Ref. 2).

Fig. 5. The same plot as Fig. 4 but showing the effect of impurities. Note the increased amount of beam power needed (from Ref. 2).

Fig. 6. Various paths in the generalized Lawson diagram for various defined scenarios explained in the text and in Ref. 2.

Fig. 7. Beta as a function of time during the approach to ignition. The curves show the beta of the electrons and ions, of the beam, and of the alphas and the total beta (from Ref. 4).

Fig. 8. The sensitivities of beta at ignition and the time needed to reach ignition as a function of variable electron heat conduction. Note the increased demand on β_{ig} and t_{ig} if the electron heat conduction is increased (from Ref. 4).

Fig. 9. Effect on ignition requirements of varying the minor plasma radius according to $a^2 \propto \chi_e$ if χ_e increases (from Ref. 4).

Fig. 10. Beta at ignition and time needed to reach ignition as a function of impurity content (from Ref. 4).

Fig. 11. Electron temperature achieved as a function of time for various levels of nickel impurity content. Note the limitations on the electron temperature for nickel concentrations larger than 0.15% (from Ref. 4).

Fig. 12. Maximum permissible (fatal) impurity fraction as a function of atomic number (from Ref. 4). The dot labeled H. Howe was obtained independently by this author.

Fig. 13. Helium fraction remaining in the plasma as a function of helium-pumping efficiency (from Ref. 4).

Fig. 14. Various plasma parameters as a function of time and radius for the approach to ignition of ETF (from Ref. 1).

Fig. 15. Extension of the Murakami density limit with auxiliary heating (from Ref. 9).

Fig. 16. Particle balance of various fluxes to the wall and divertor in ETF (from Ref. 1).

Fig. 17. Energy balance of various quantities going to the wall and divertor in ETF (from Ref. 1).

Fig. 18. Overall fusion power as a function of time (from Ref. 1).

Fig. 19. Ripple losses in ETF; δ_0 is the ripple strength. Injection angle is 2.5° from vertical (from Ref. 8).

Fig. 20. Ripple losses in ETF; δ_0 is the ripple strength. Injection angle is 16° from vertical (from Ref. 8).

Fig. 21. Beam power loss as a function of injection angle measured by the tangency radius. P1, P2, and P3 refer to a set of plasma parameters; q_3 means safety factor at the edge = 3, etc. δ is the ripple strength (from Ref. 8).

Fig. 22. Schematic of alpha particle diagnostic experiment (after D. Post, Ref. 15).

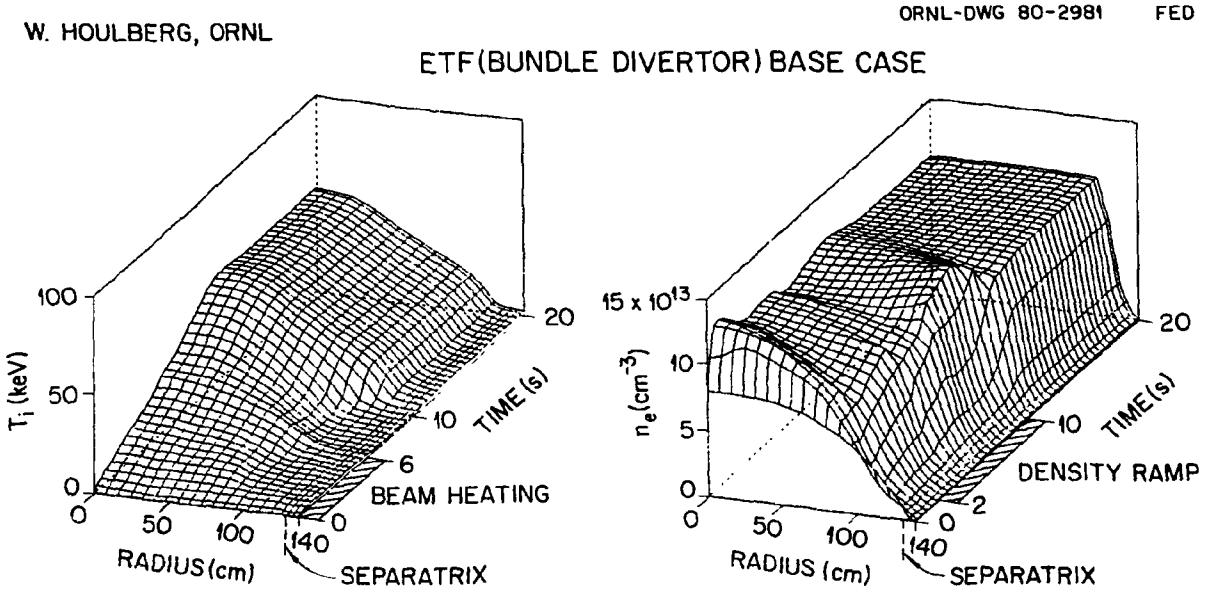
W. HOULBERG, ORNL
ORNL-DWG 80-2981 FED
ETF(BUNDLE DIVERTOR) BASE CASE
100
50
0
T_i (keV)
0
50
100
140
RADIUS (cm)
SEPARATRIX
0
6
10
20
TIME (s)
BEAM HEATING
15 x 10^{13}
10
5
0
n_e (cm^{-3})
0
50
100
140
RADIUS (cm)
SEPARATRIX
0
2
10
20
TIME (s)
DENSITY RAMP

Fig. 1

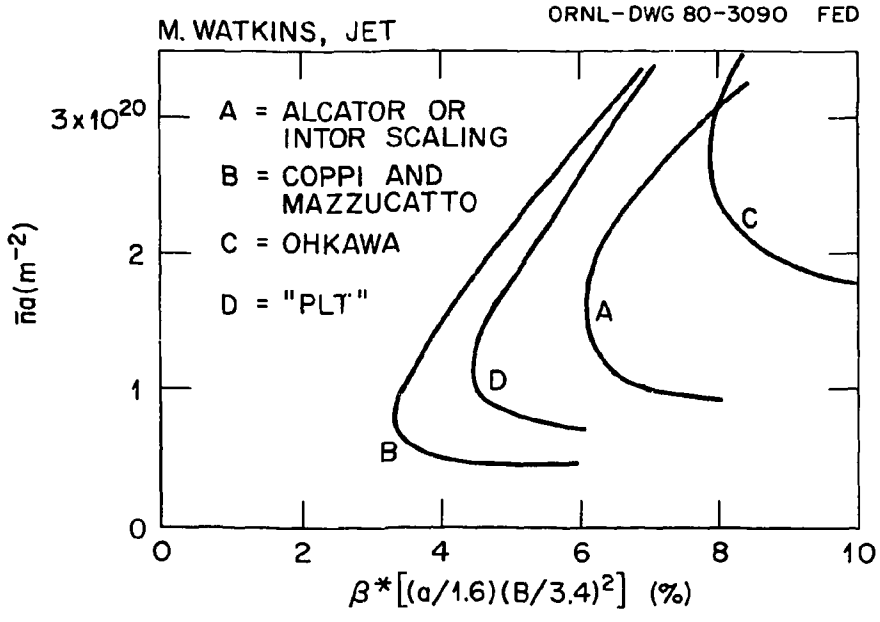
M. WATKINS, JET
ORNL-DWG 80-3090 FED
A = ALCATOR OR INTOR SCALING
B = COPPI AND MAZZUCATTO
C = OHKAWA
D = "PLT"
3×10^{20}
2
1
0
$\bar{n}a(m^{-2})$
0
2
4
6
8
10
$\beta^*[(a/1.6)(B/3.4)^2]$ (%)

Fig. 2

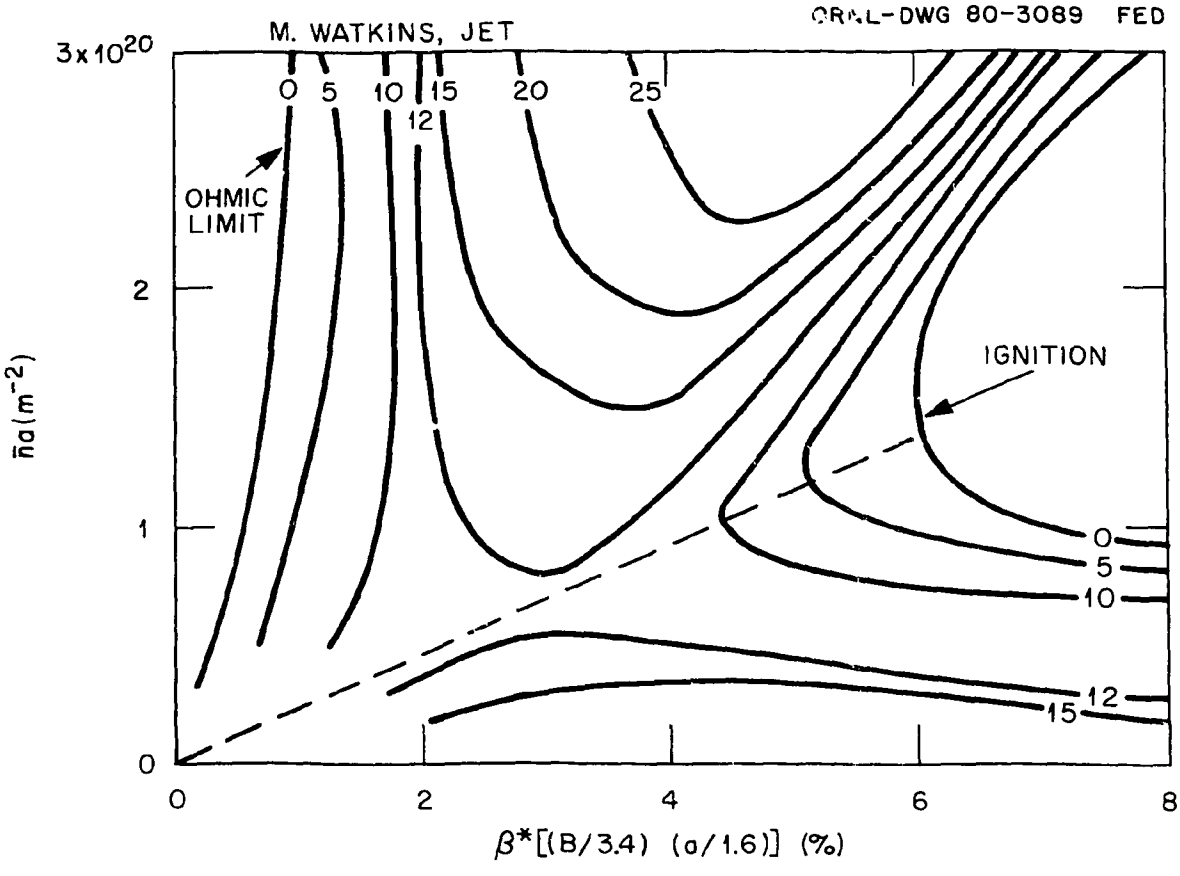
M. WATKINS, JET
ORNL-DWG 80-3089 FED
3x10^20
0
5
10
15
12
20
25
OHMIC LIMIT
IGNITION
2
1
0
0
5
10
12
15
0
2
4
6
8
β*[(B/3.4) (a/1.6)] (%)
n̄a(m^-2)

Fig. 3

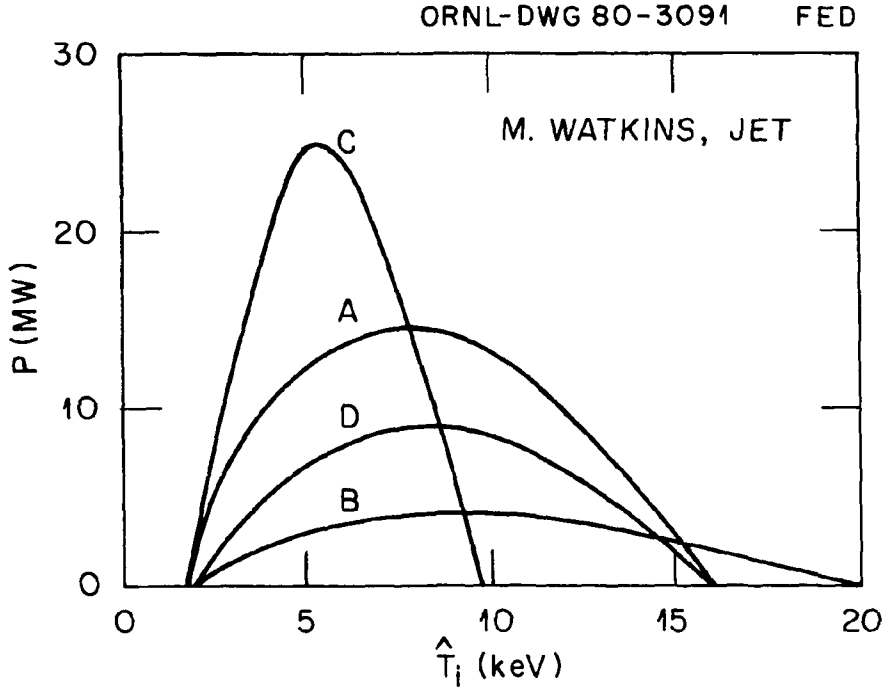
ORNL-DWG 80-3091 FED
M. WATKINS, JET
C
A
D
B
P (MW)
30
20
10
0
0
5
10
15
20
$\hat{T}_i$ (keV)

Fig. 4

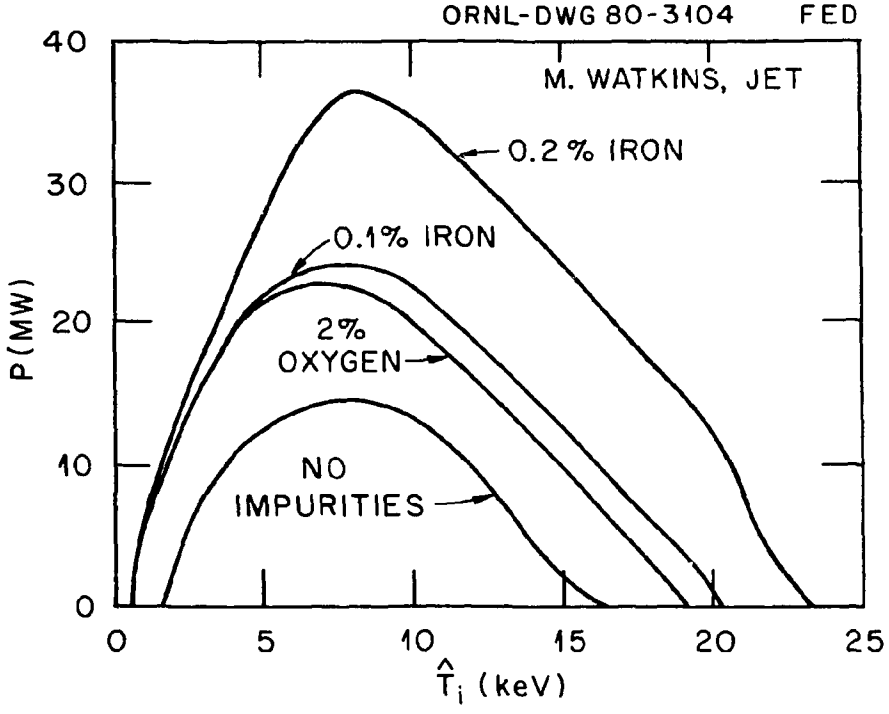
ORNL-DWG 80-3104 FED
M. WATKINS, JET
0.2 % IRON
0.1% IRON
2%
OXYGEN
NO
IMPURITIES
P(MW)
40
30
20
10
0
0
5
10
15
20
25
$\hat{T}_i$ (keV)

Fig. 5

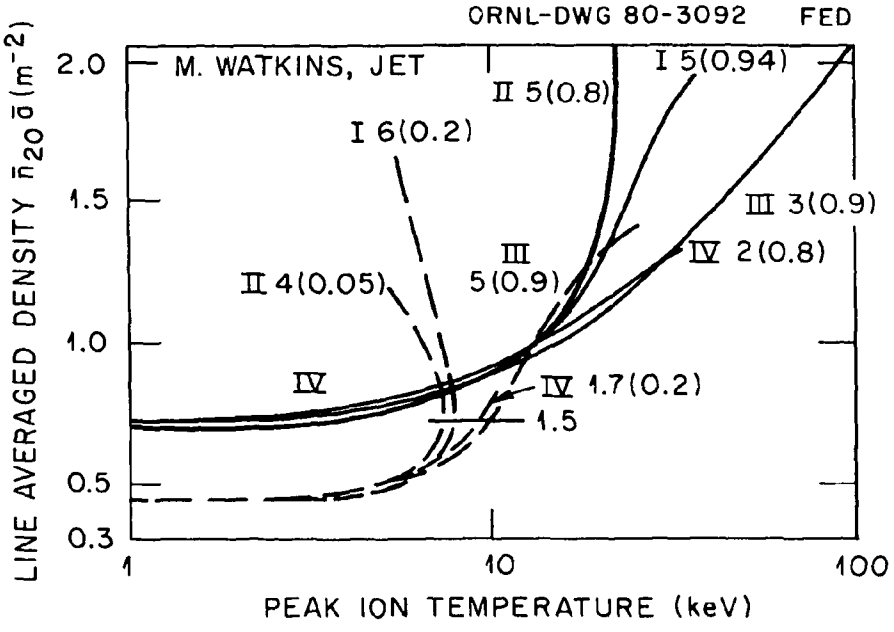
ORNL-DWG 80-3092 FED
M. WATKINS, JET
I 5(0.94)
II 5(0.8)
I 6(0.2)
III 3(0.9)
III 5(0.9)
IV 2(0.8)
II 4(0.05)
IV
IV 1.7(0.2)
1.5
2.0
1.5
1.0
0.5
0.3
1
10
100
LINE AVERAGED DENSITY $\bar{n}_{20}\bar{a}\,(m^{-2})$
PEAK ION TEMPERATURE (keV)

Fig. 6

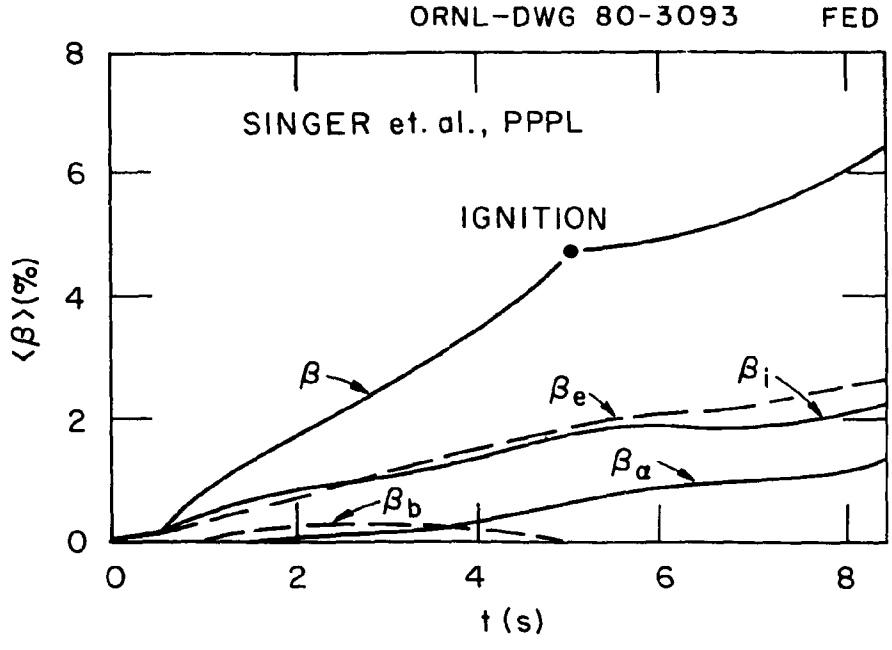
ORNL-DWG 80-3093 FED
SINGER et. al., PPPL
IGNITION
⟨β⟩(%)
t (s)
β
βe
βi
βα
βb
0
2
4
6
8

Fig. 7

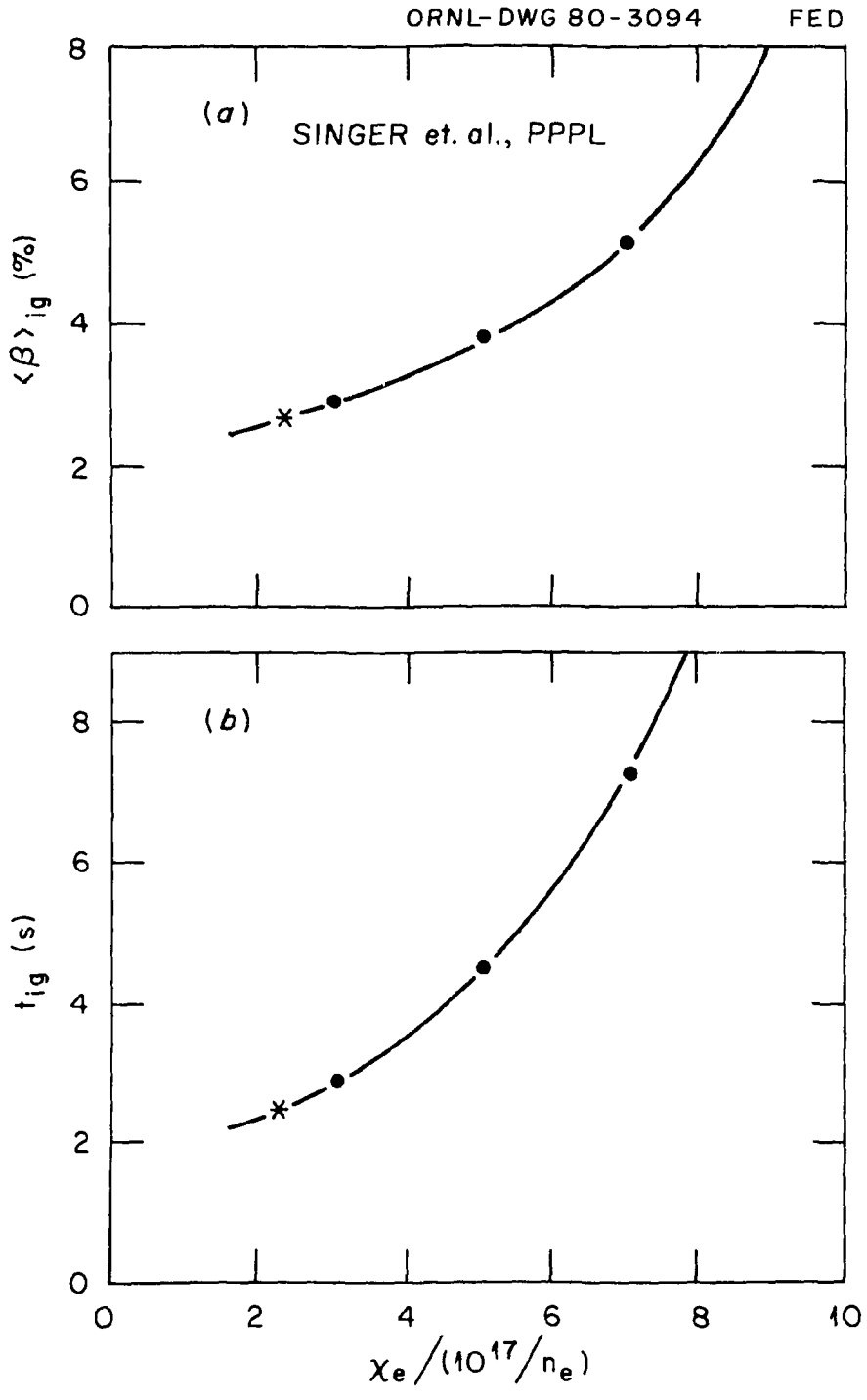
ORNL-DWG 80-3094 FED
(a)
SINGER et. al., PPPL
$\langle\beta\rangle_{ig}$ (%)
(b)
t_{ig} (s)
$\chi_e/(10^{17}/n_e)$
0
2
4
6
8
10

Fig. 8

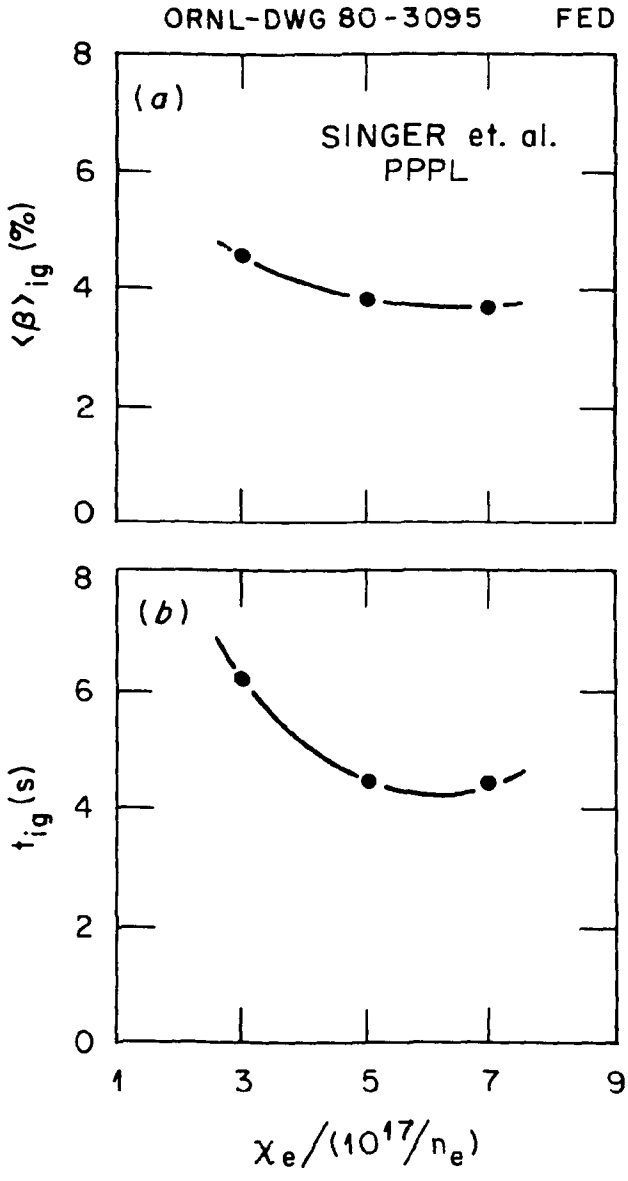

a_{eq}(m)	1.14	1.47	1.74
R(m)	4.53	4.80	5.02
B(m)	5.30	5.00	4.78
I_{eq}(MA)	2.37	3.75	4.44
P_b(MW)	34	60	88

CLOSE TO ETF

Fig. 9

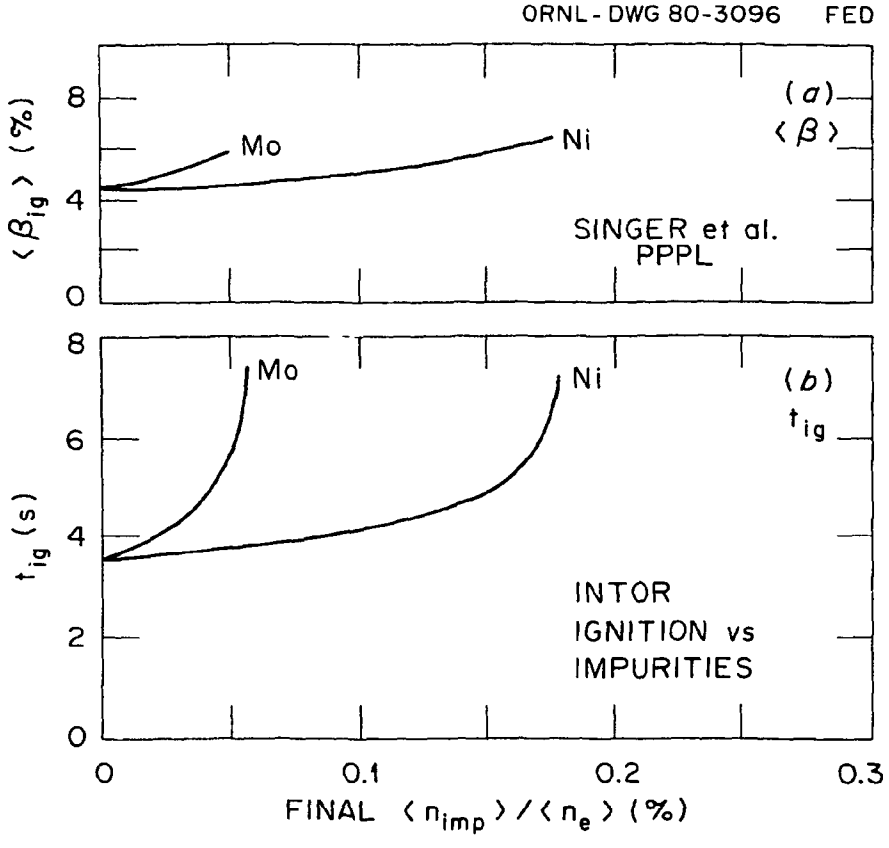
ORNL-DWG 80-3096 FED
(a)
⟨β⟩
Mo
Ni
SINGER et al.
PPPL
⟨β_ig⟩ (%)
8
4
0
(b)
t_ig
Mo
Ni
INTOR
IGNITION vs
IMPURITIES
t_ig (s)
8
6
4
2
0
0
0.1
0.2
0.3
FINAL ⟨n_imp⟩/⟨n_e⟩ (%)

Fig. 10

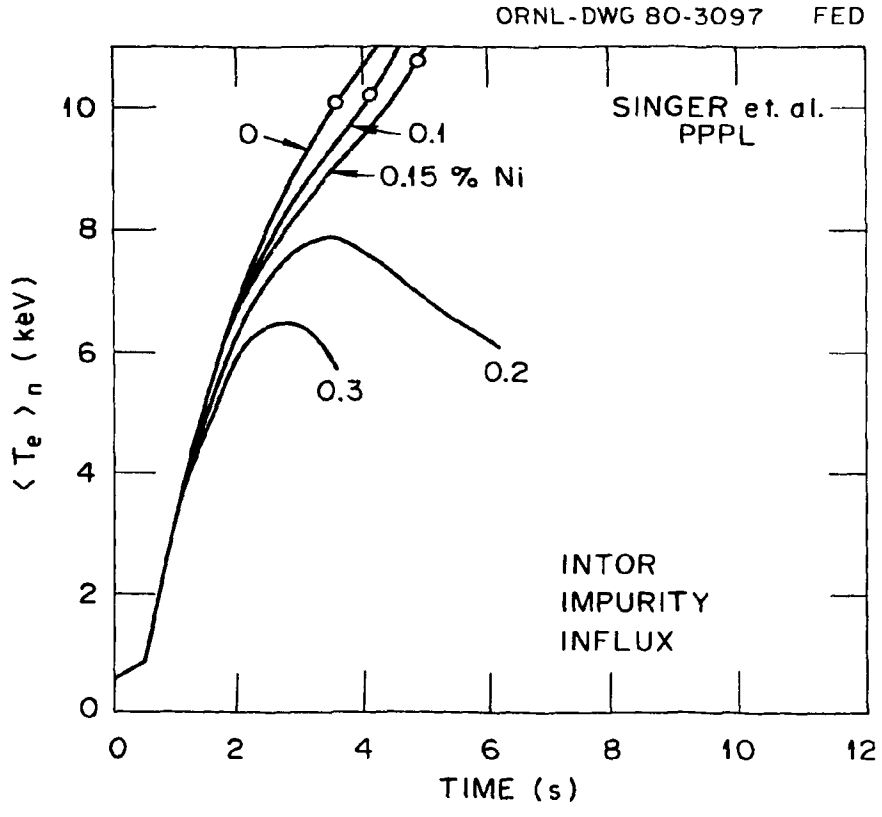
ORNL-DWG 80-3097 FED
SINGER et. al.
PPPL
0
0.1
0.15 % Ni
0.2
0.3
INTOR
IMPURITY
INFLUX
$\langle T_e \rangle_n$ (keV)
TIME (s)
0
2
4
6
8
10
12

Fig. 11

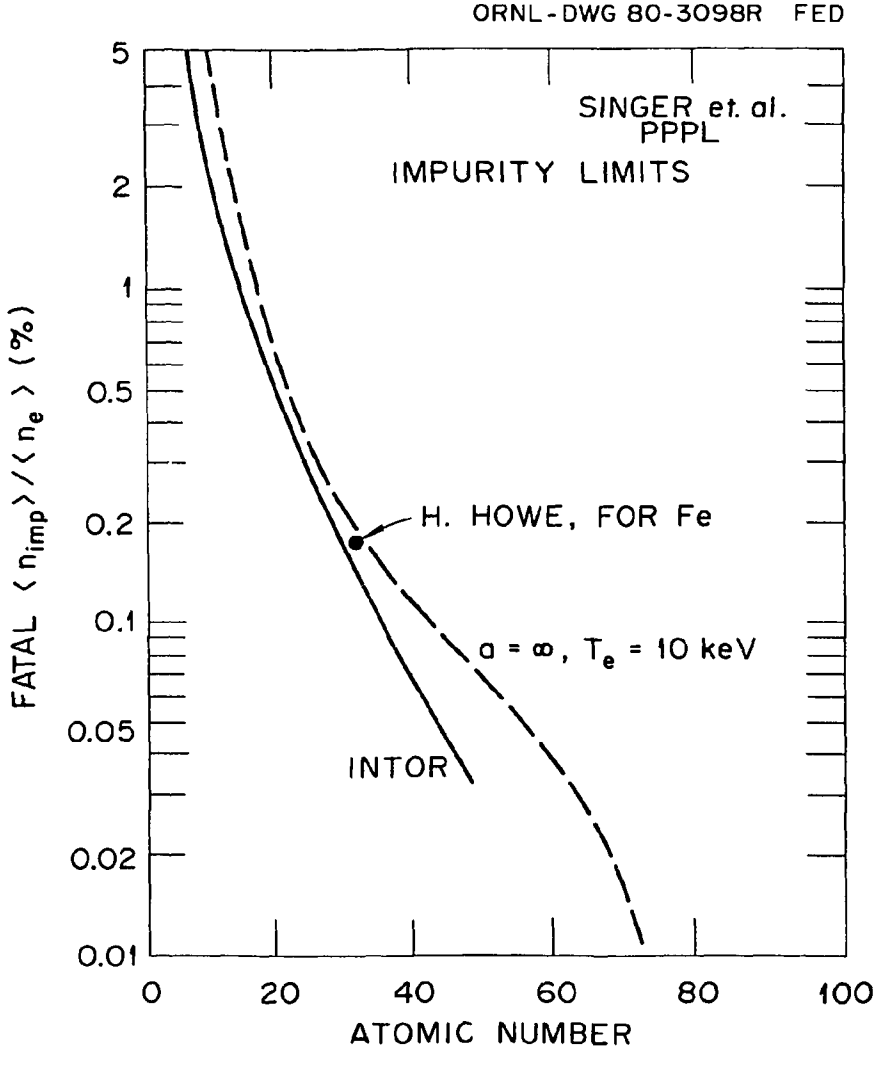
ORNL-DWG 80-3098R FED
SINGER et. al.
PPPL
IMPURITY LIMITS
H. HOWE, FOR Fe
a = ∞, T_e = 10 keV
INTOR
FATAL $\langle n_{imp} \rangle / \langle n_e \rangle$ (%)
ATOMIC NUMBER
5
2
1
0.5
0.2
0.1
0.05
0.02
0.01
0
20
40
60
80
100

Fig. 12

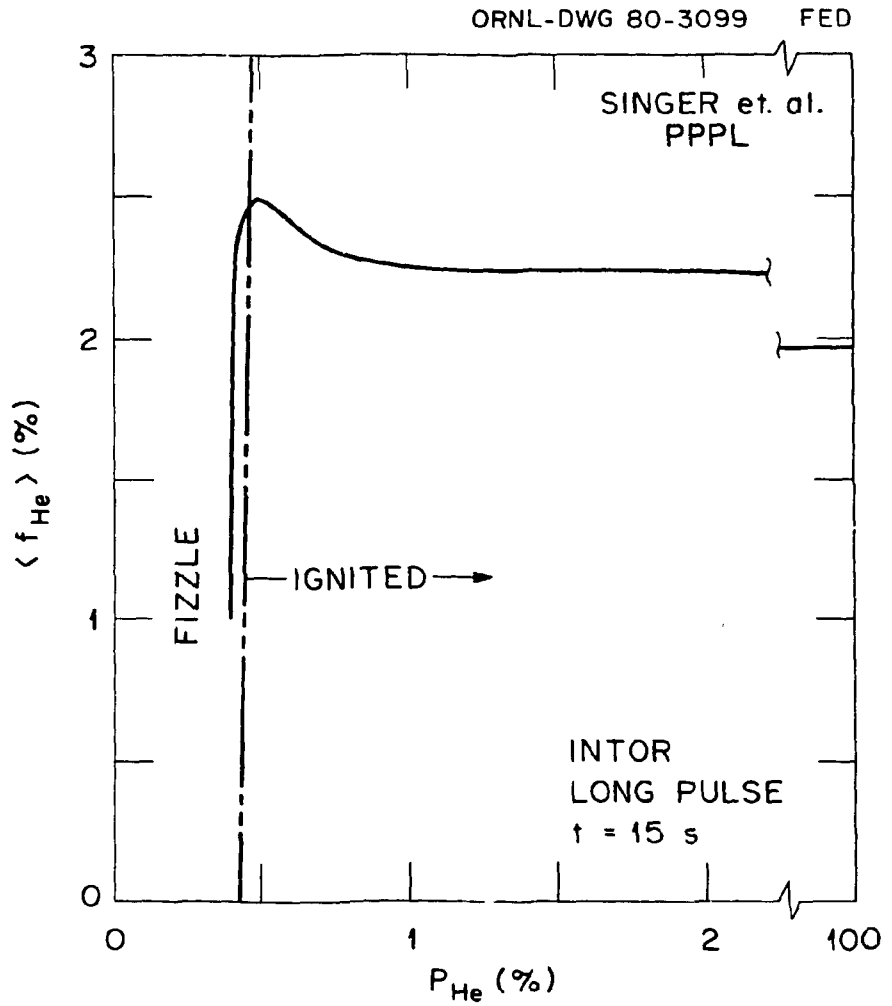
ORNL-DWG 80-3099 FED
SINGER et. al.
PPPL
FIZZLE
IGNITED
INTOR
LONG PULSE
t = 15 s
⟨ f He ⟩ (%)
P He (%)
0
1
2
3
0
1
2
100

Fig. 13

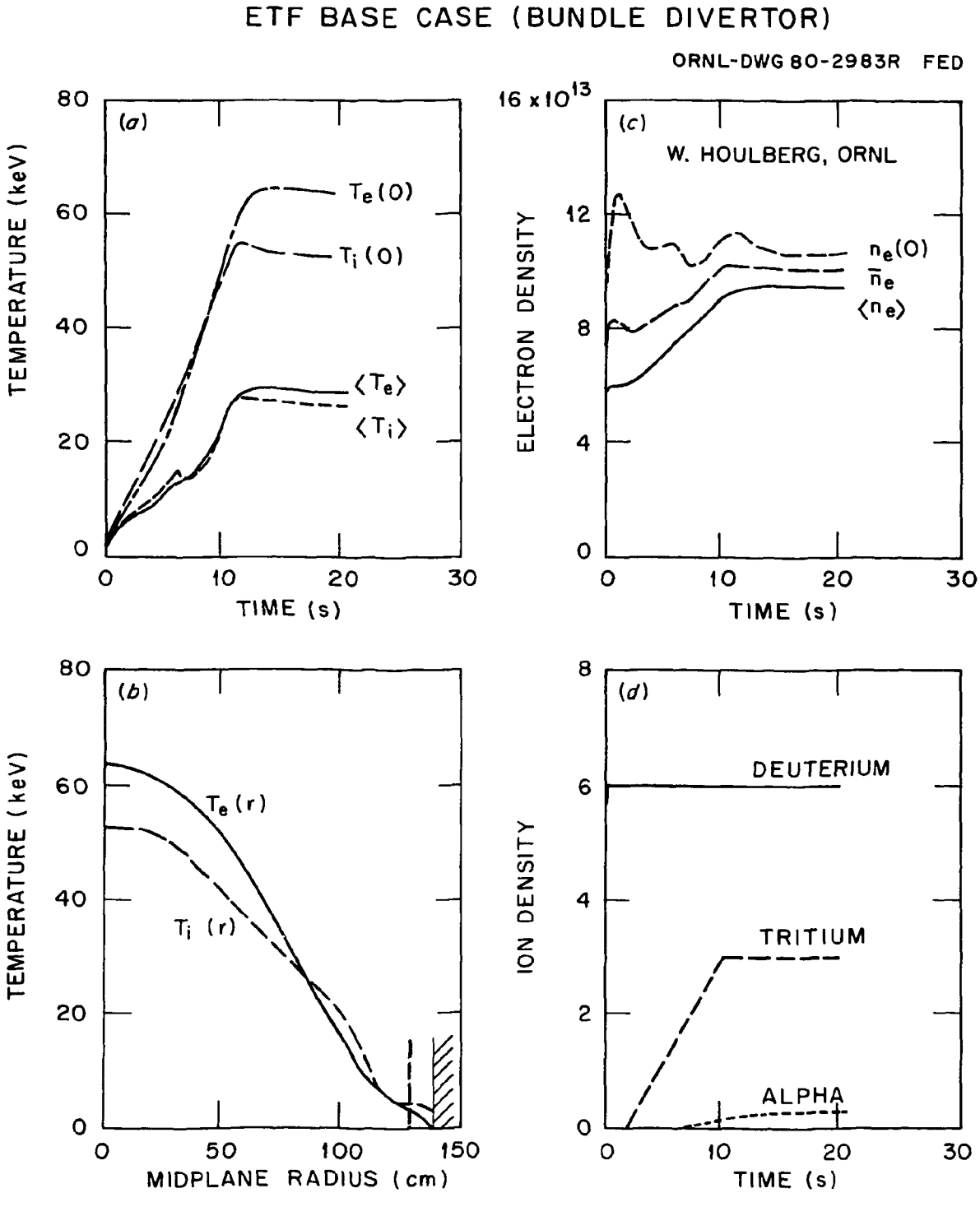
ETF BASE CASE (BUNDLE DIVERTOR)
ORNL-DWG 80-2983R FED
(a)
TEMPERATURE (keV)
$T_e(0)$
$T_i(0)$
$\langle T_e \rangle$
$\langle T_i \rangle$
TIME (s)
(c)
W. HOULBERG, ORNL
16×10^{13}
ELECTRON DENSITY
$n_e(0)$
$\bar{n}_e$
$\langle n_e \rangle$
TIME (s)
(b)
TEMPERATURE (keV)
$T_e(r)$
$T_i(r)$
MIDPLANE RADIUS (cm)
(d)
ION DENSITY
DEUTERIUM
TRITIUM
ALPHA
TIME (s)

Fig. 14

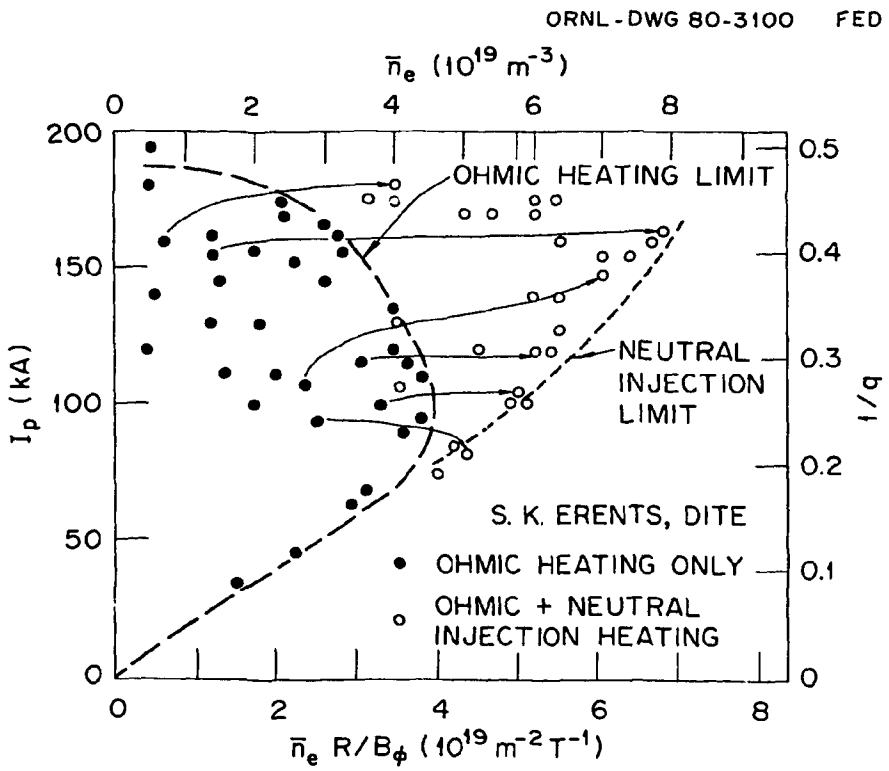
ORNL-DWG 80-3100 FED
$\bar{n}_e$ (10^{19} m^{-3})
0
2
4
6
8
200
150
100
50
0
I_p (kA)
0.5
0.4
0.3
0.2
0.1
0
1/q
OHMIC HEATING LIMIT
NEUTRAL INJECTION LIMIT
S. K. ERENTS, DITE
OHMIC HEATING ONLY
OHMIC + NEUTRAL INJECTION HEATING
$\bar{n}_e$ R/B$_\phi$ (10^{19} m^{-2} T^{-1})

Fig. 15

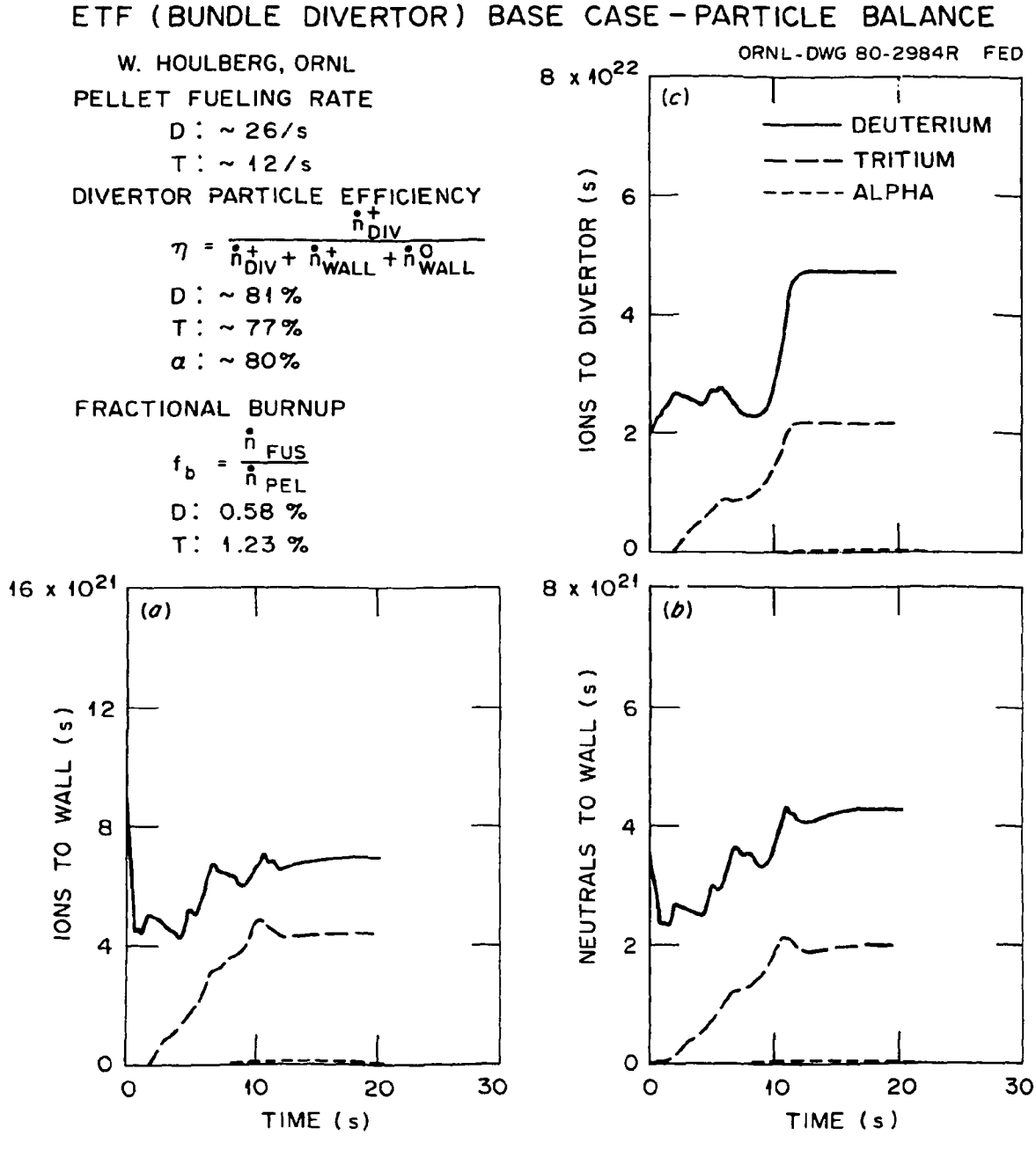
ETF (BUNDLE DIVERTOR) BASE CASE - PARTICLE BALANCE
W. HOULBERG, ORNL
PELLET FUELING RATE
D : ~ 26/s
T : ~ 12/s
DIVERTOR PARTICLE EFFICIENCY
$\eta = \frac{\dot{n}^{+}_{DIV}}{\dot{n}^{+}_{DIV} + \dot{n}^{+}_{WALL} + \dot{n}^{0}_{WALL}}$
D : ~ 81 %
T : ~ 77 %
α : ~ 80 %
FRACTIONAL BURNUP
$f_b = \frac{\dot{n}_{FUS}}{\dot{n}_{PEL}}$
D: 0.58 %
T: 1.23 %
ORNL-DWG 80-2984R FED
8 x 10^22
(c)
DEUTERIUM
TRITIUM
ALPHA
IONS TO DIVERTOR (s)
0
2
4
6
16 x 10^21
(a)
IONS TO WALL (s)
0
4
8
12
0
10
20
30
TIME (s)
8 x 10^21
(b)
NEUTRALS TO WALL (s)
0
2
4
6
0
10
20
30
TIME (s)

Fig. 16

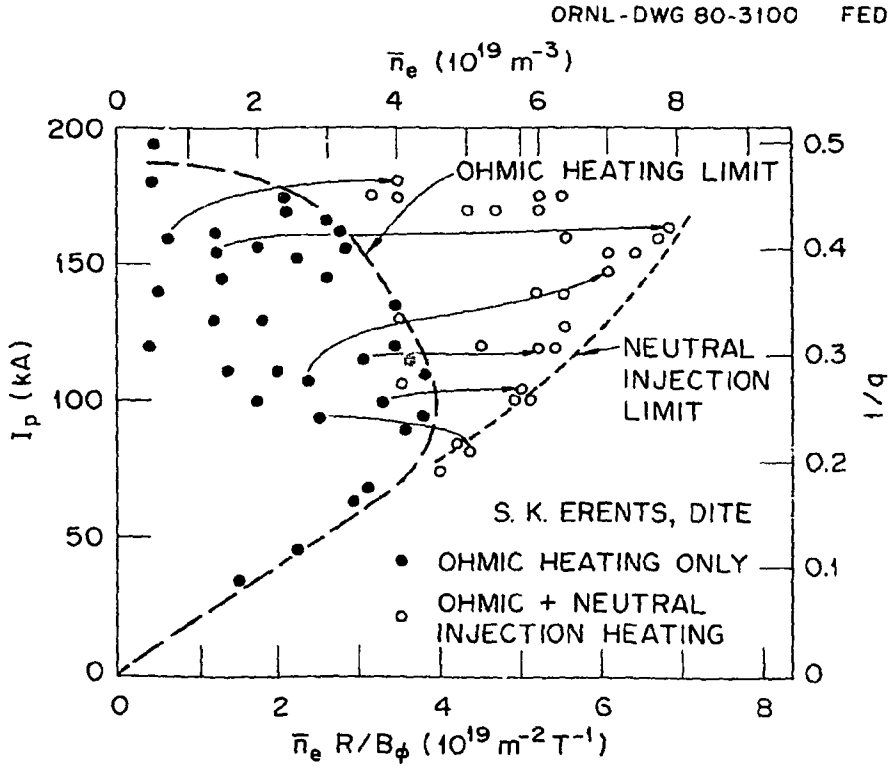
ORNL-DWG 80-3100 FED
$\bar{n}_e$ (10^{19} m^{-3})
0
2
4
6
8
200
150
100
50
0
I_p (kA)
0.5
0.4
0.3
0.2
0.1
0
1/q
OHMIC HEATING LIMIT
NEUTRAL INJECTION LIMIT
S. K. ERENTS, DITE
OHMIC HEATING ONLY
OHMIC + NEUTRAL INJECTION HEATING
$\bar{n}_e$ R/B$_\phi$ (10^{19} m^{-2} T^{-1})

Fig. 15

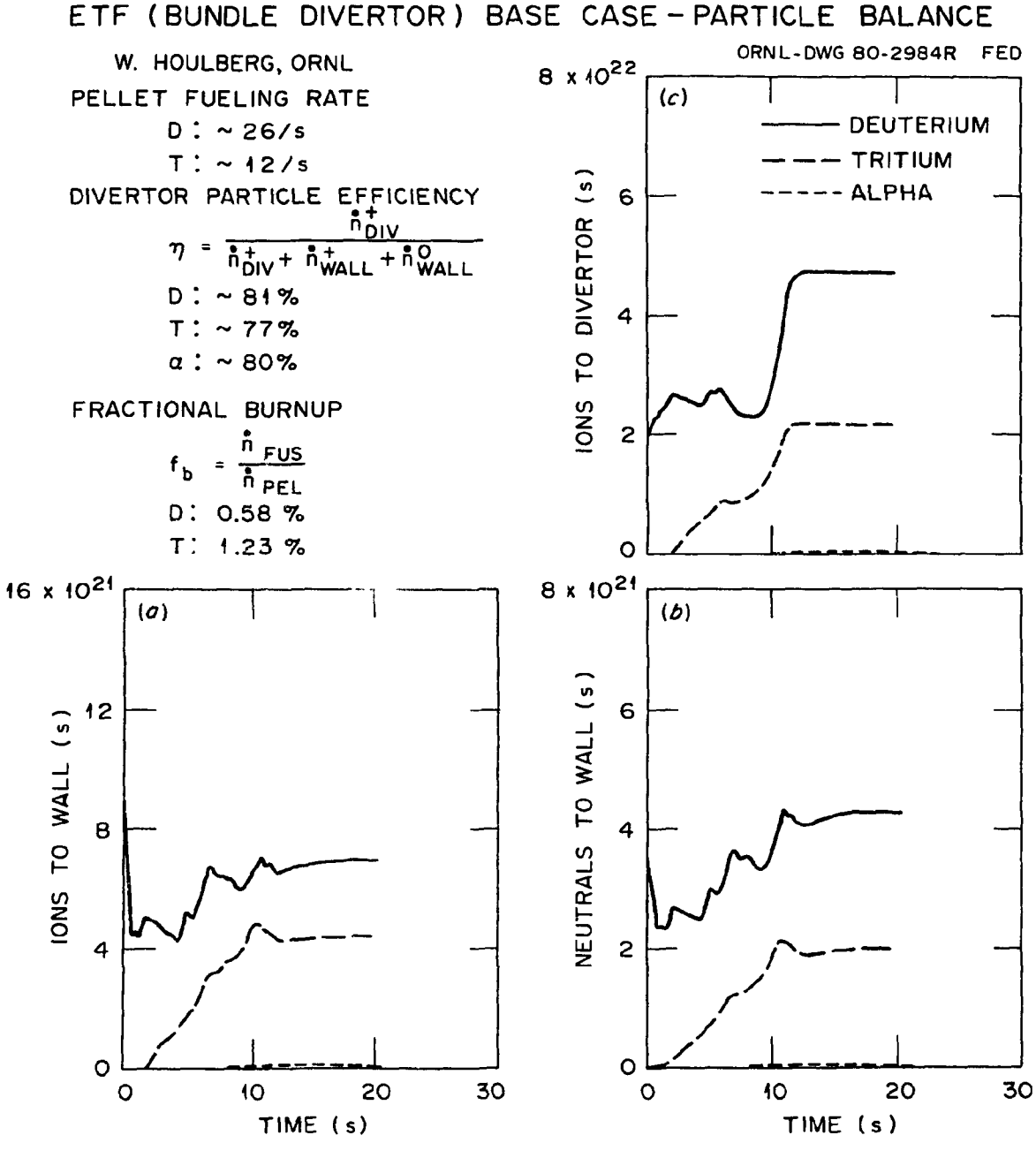
ETF (BUNDLE DIVERTOR) BASE CASE - PARTICLE BALANCE
W. HOULBERG, ORNL
ORNL-DWG 80-2984R FED
PELLET FUELING RATE
D : ~ 26/s
T : ~ 12/s
DIVERTOR PARTICLE EFFICIENCY
$\eta = \frac{\dot{n}^{+}_{DIV}}{\dot{n}^{+}_{DIV} + \dot{n}^{+}_{WALL} + \dot{n}^{0}_{WALL}}$
D : ~ 81%
T : ~ 77%
α : ~ 80%
FRACTIONAL BURNUP
$f_b = \frac{\dot{n}_{FUS}}{\dot{n}_{PEL}}$
D: 0.58 %
T: 1.23 %
8 x 10^22
(c)
DEUTERIUM
TRITIUM
ALPHA
IONS TO DIVERTOR (s)
0
2
4
6
16 x 10^21
(a)
IONS TO WALL (s)
0
4
8
12
0
10
20
30
TIME (s)
8 x 10^21
(b)
NEUTRALS TO WALL (s)
0
2
4
6
0
10
20
30
TIME (s)

Fig. 16

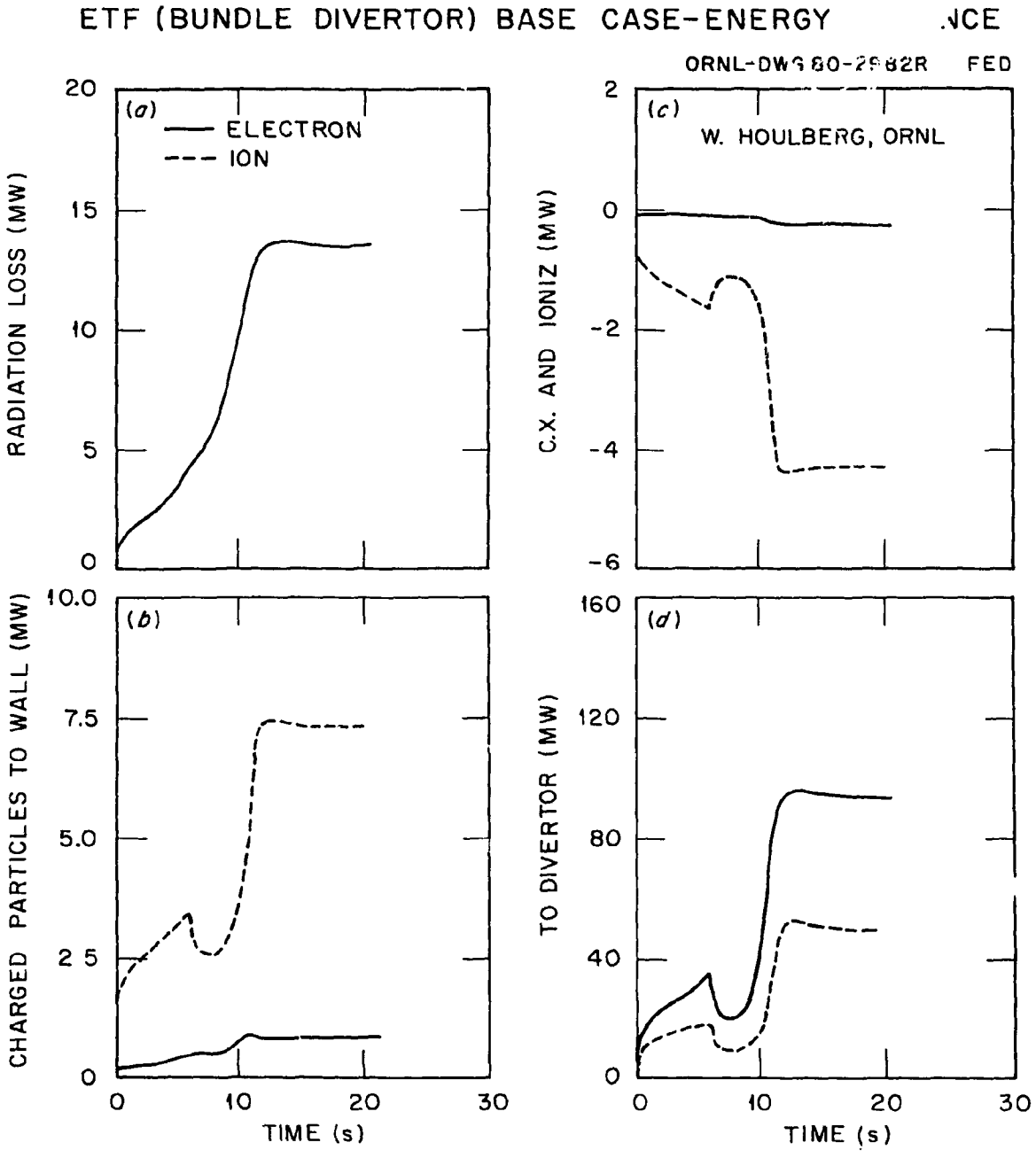
ETF (BUNDLE DIVERTOR) BASE CASE-ENERGY .NCE
ORNL-DWG 80-2982R FED
(a)
ELECTRON
ION
RADIATION LOSS (MW)
20
15
10
5
0
(c)
W. HOULBERG, ORNL
C.X. AND IONIZ (MW)
2
0
-2
-4
-6
(b)
CHARGED PARTICLES TO WALL (MW)
10.0
7.5
5.0
2 5
0
(d)
TO DIVERTOR (MW)
160
120
80
40
0
0
10
20
30
TIME (s)
0
10
20
30
TIME (s)

Fig. 17

ETF (BUNDLE DIVERTOR) BASE CASE — ENERGY BALANCE

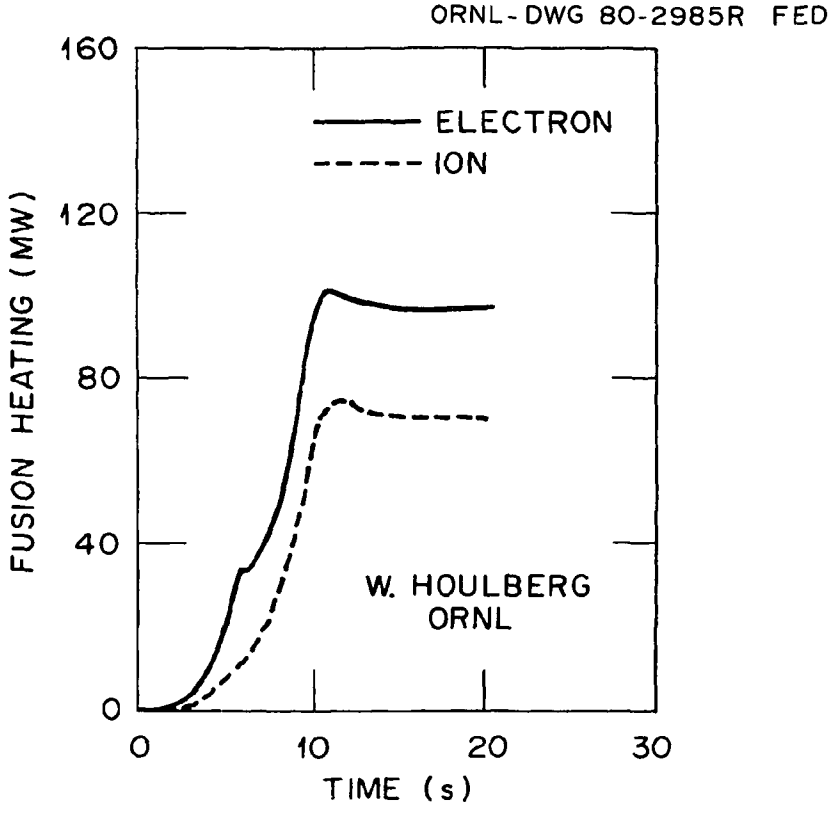

P_{FUS} = 835 MW (INTOR 625 MW)

P_{α} = 167 MW (INTOR 125 MW)

A_{WALL} = 320 m^2

DIVERTOR ENERGY EFFICIENCY (NO IMPURITIES)

OVERALL : $\eta_T = \frac{P_{DIV}}{P_{\alpha}} = 84.4\ \%$

PARTICLE : $\eta_P = \frac{P_{DIV}}{P_{\alpha} - P_{RAD}} = 91.9\ \%$

Fig. 18

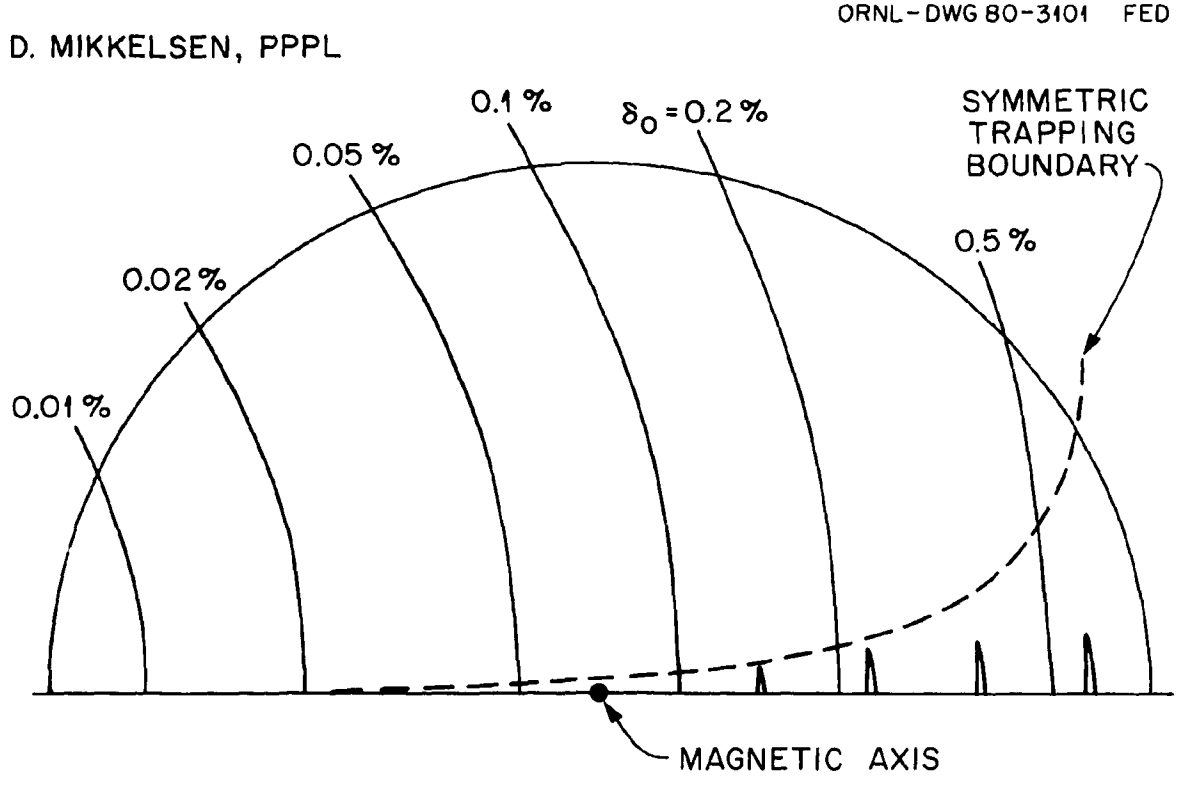
ORNL-DWG 80-3101 FED
D. MIKKELSEN, PPPL
0.1 %
δ_0 = 0.2 %
SYMMETRIC
TRAPPING
BOUNDARY
0.05 %
0.5 %
0.02 %
0.01 %
MAGNETIC AXIS

Fig. 19

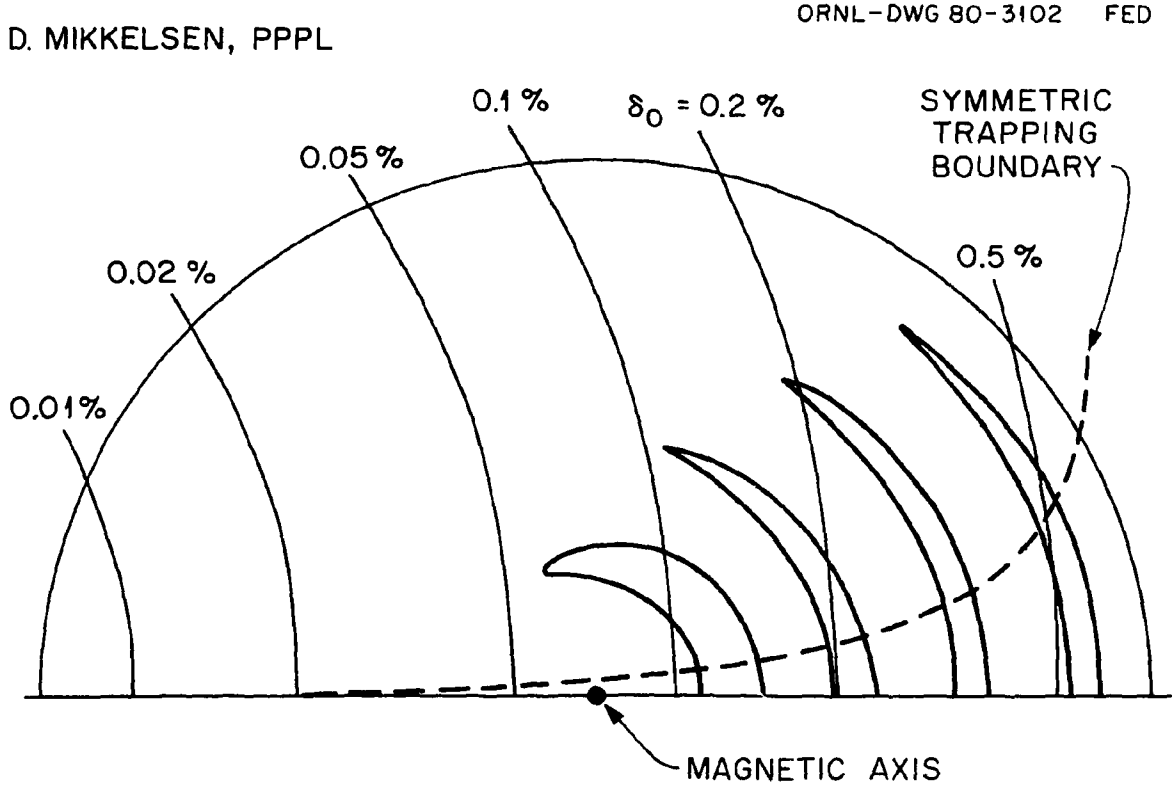
D. MIKKELSEN, PPPL
ORNL-DWG 80-3102 FED
0.1 %
δ_0 = 0.2 %
SYMMETRIC
TRAPPING
BOUNDARY
0.05 %
0.5 %
0.02 %
0.01%
MAGNETIC AXIS

Fig. 20

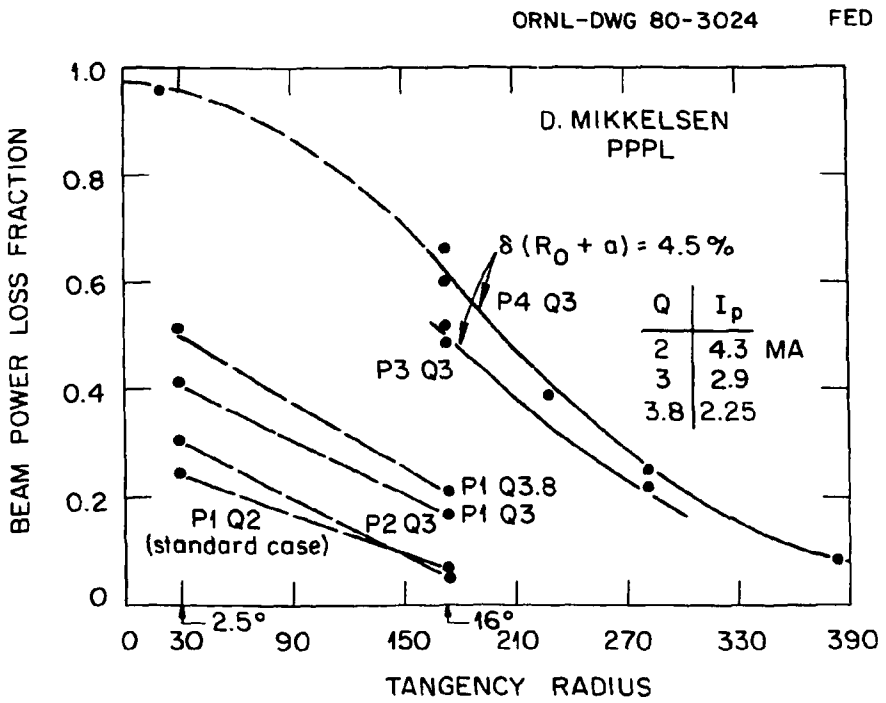
ORNL-DWG 80-3024 FED
D. MIKKELSEN
PPPL
BEAM POWER LOSS FRACTION
TANGENCY RADIUS
1.0
0.8
0.6
0.4
0.2
0
0 30 90 150 210 270 330 390
2.5°
16°
δ (R0 + a) = 4.5 %
P4 Q3
P3 Q3
P1 Q3.8
P1 Q3
P2 Q3
P1 Q2
(standard case)
Q | Ip
2 | 4.3 MA
3 | 2.9
3.8 | 2.25

Fig. 21

D. POST, PPPL

ORNL-DWG 80-3103 FED

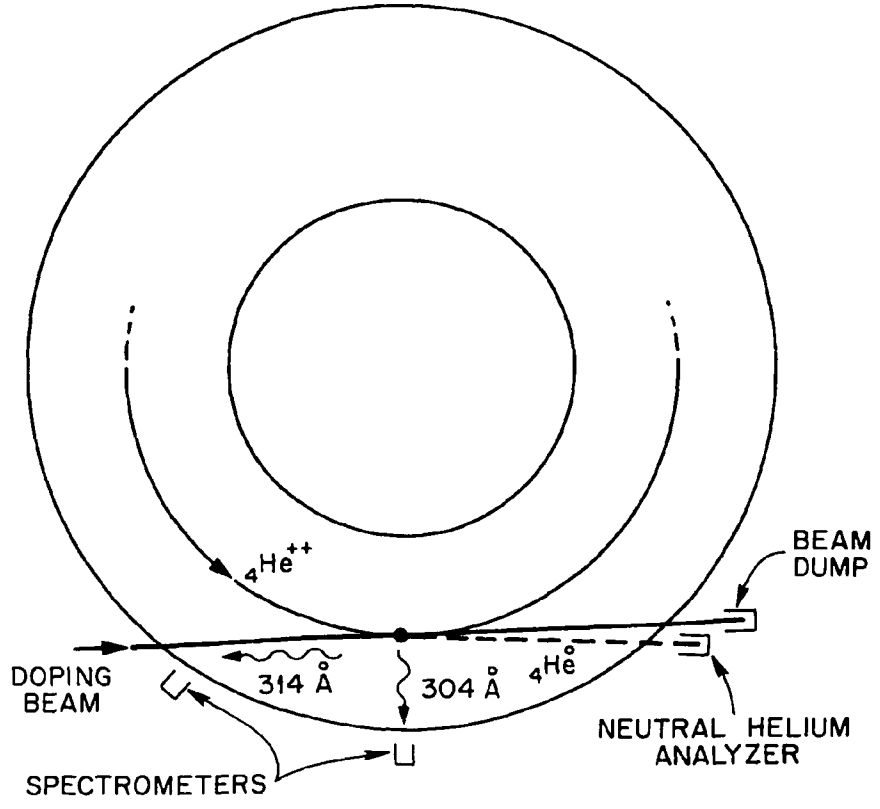

Fig. 22